Thermodynamic approach to rheology of complex fluids: Flow-concentration coupling

B. García-Rojas,[1] F. Bautista,[2] J. E. Puig,[2] and O. Manero[1,*]
[1]*Instituto de Investigaciones en Materiales & Facultad de Química, UNAM, A.P. 70-360, México, Distrito Federal 04510, Mexico*
[2]*Departamentos de Física & Ingeniería Química, Universidad de Guadalajara, Boulevard M. García Barragán 1451, Guadalajara, Jal 44430, Mexico*
(Received 18 February 2009; revised manuscript received 29 April 2009; published 22 September 2009)

In this work, the generalized *Bautista-Manero-Puig* (BMP) model derived from extended irreversible thermodynamics (EIT) is used to analyze the coupling of stress with concentration in complex fluids. It is shown that this model is consistent with previous analyses that predict mechanical and thermodynamic instabilities in the shear-banding regime. In particular, for simple shear flows, the model presented here predicts the structure factor in the plane of shear and the onset of instabilities in the gradient-vorticity plane. Furthermore, the model predicts distinctive features of the models of Brochard–de Gennes and Schmitt *et al.* as particular cases. For finite stress relaxation time, the generalized BMP model allows the prediction of transient structures normal to the vorticity axis. Instabilities are predicted in the regions of high viscosity, which suggest that the induction of a more viscous phase in a shear-thickening solution can lead the system to instability, in this case, the layering is predicted perpendicular to the vorticity direction. These transient structural patterns within the shear-thickening region correspond to spinodal phase separation. When the mechanical and thermodynamic instabilities are uncoupled, the model predictions agree with experiments and with the transient-gel model of Brochard and de Gennes.

DOI: 10.1103/PhysRevE.80.036313 PACS number(s): 47.20.−k, 47.50.−d, 83.80.Qr, 83.10.−y

I. INTRODUCTION

In recent years, much attention has focused on complex fluids, in which a certain internal structure of the fluid is strongly affected by a flow field (see, for example, a general review of material instability in complex fluids, by Goddard [1]). Experimentally, the research has been done through the application of scattering techniques to nonequilibrium phenomena under shear. Birefringence and dichroism combined with rheomechanical data have also been used for sensitive detection of the spatial anisotropy arising from composition fluctuations and molecular alignment in complex flows. Hence the prediction of the associated structure factor is a key issue of theoretical modeling.

Analogously to critical liquid-gas behavior of simple liquids, shear flow causes a thermal shift in the critical point [2]. The flow of complex fluids, like wormlike micelles, polymer and surfactants solutions, or emulsions, can modify or induce phase transitions, such as the de-mixing transition found in high molecular weight polymer solutions [3]. One explanation of these changes in the critical point is based on a coupling of stress with order parameter fluctuations near the phase transition [4]. Shear flow suppresses those fluctuations with characteristic times larger than reciprocal of the shear rate. Generally speaking, in a simple liquid near the gas-liquid transition, such slow modes tend to be longer wavelength fluctuations characteristic of critical behavior, and hence, the suppression of these fluctuations shifts the critical point to lower temperatures. By contrast, in the de-mixing of polymer solutions, stress enhances critical fluctuations and raises the de-mixing temperature [5].

Complex fluids show a variety of flow phenomena such as flow-induced phase transitions and instabilities [6–9]. These systems are characterized by a nonmonotonic relation between the shear stress, σ_{12}, and the shear rate, $\dot{\gamma}_{12}$ [10–12], where the subscripts 1, 2, and 3 indicate the velocity, velocity gradient, and vorticity directions, respectively. As indicated elsewhere, this kind of flow curve exhibits a constant shear stress with at least two values of shear rate [13–18]. Consequently, the flow is nonhomogeneous and each phase is supporting a different shear rate. In the banded regime, changes in shear rate essentially alter the proportion of the low and high viscosity bands and the initially homogeneous flow becomes mechanically unstable.

The kinetics of formation of inhomogeneous flows in the plateau stress range has distinctive features. The characteristic time for the sigmoidal evolution of the stress toward a steady-state plateau was found to be much longer than the reptation time. According to Porte *et al.* [19], such kinetics is typical of a nucleation-and-growth process, usually associated with first-order phase transitions. In some systems, the nucleation-and-growth process leads to a kind of spinodal instability [20].

The models derived from a criterion of complete mechanical instability, corresponding to a negative slope in the flow curve and in which the medium separates into a fluid phase of high shear rate and a viscous phase of low shear rate (the so-called shear-banding instability), sometimes disagree with experimental data. It has been observed that the fluid phase often nucleates in the region of shear rates smaller than the critical shear rates that bound the negative slope region, i.e., before the criterion of mechanical instability is reached. In this regard, both approaches, mechanical instability and nonequilibrium phase transition, are not incompatible.

To incorporate nonequilibrium phase transitions and rheologically driven instabilities, some theories have been forwarded, such as that of Schmitt *et al.* [21]. These authors proposed a classification scheme for the instabilities arising

*Corresponding author; manero@servidor.unam.mx

from the coupling between flow and concentration, based on a combination of parameters describing the tendency of solute molecules to migrate to regions of small or high shear rates and the variation in viscosity with concentration.

In this work, the generalized Bautista-Manero-Puig (BMP) model is used to predict the instability regions for simple shear in the plane of shear and in the gradient-vorticity plane. The coupling of flow with concentration naturally arises from the thermodynamic framework, such that the constitutive equations for the stress, mass flux, and the evolution equation for structural changes are all coupled each other to lowest order. The paper analyzes two general situations: in the first one, the calculation of the structure factor in the plane of shear is carried out, allowing fluctuations in concentration and stress, wherein the chemical potential is a function of velocity gradient and concentration. The assumed dependence of chemical potential on velocity gradient allows for a diffusional driving force between regions of different deformation rate. In the second one, fluctuations in the velocity are considered, and a generalization of the model of Schmitt *et al.* is achieved by including stress relaxation. In this case, the scattering vector lies in the gradient-vorticity plane. Detailed numerical and analytical predictions of instability regions along the flow curve of a cationic wormlike micellar solution [cetyltrimethylammonium tosilate (CTAT)] are exposed.

The paper is structured as follows. In Sec. I, a brief review of the relevant models for the flow-concentration coupling is presented. In Sec. II, the generalized BMP model with small departures from equilibrium (within the Newtonian region) is used to analyze the stress-concentration coupling with the chemical potential being a function of both concentration and shear rate. In Sec. III, shear rate sweeps along the intrinsic constitutive curve are considered to determine the onset for instabilities. In Sec. IV, results for uncoupled and coupled models are presented. Finally, in Sec. V, the concluding remarks are given.

II. PAST MODELING OF FLOW-CONCENTRATION COUPLING

Shear-enhanced concentration fluctuations around the nonequilibrium critical point (located at the onset of the plateau in the shear stress) can be explained by the coupling of stress with concentration. This coupling in a transient gel was first explored theoretically by Brochard and de Gennes [22]. A transient gel behaves as a simple two-fluid mixture on time scales long comparable to the stress relaxation time, but it behaves as a solvated gel on short time scales. The coupling of stress with concentration causes the growth of concentration fluctuations observed in the experiments. The concept of *transient gel* within a two-fluid mixture has been the framework to later extensions to the Helfand-Fredrickson theory [3], namely, those of Doi and Onuki [23] and Milner [24,25]. In these models, the stress relaxation time is introduced in the constitutive equations.

The Brochard–de Gennes model predicts two modes for the stress relaxation of the transient gel. At small wave numbers ($\bar{k}$), all the weight is in the slowly decaying mode, while at large $\bar{k}$, the fast and slow decay rates have comparable weights when the plateau and the osmotic moduli are comparable. The light-scattering signal (for a fixed $\bar{k}$) as a function of frequency (ω) is the sum of two Lorentzians: a narrow Lorentzian of half-width Ω_s and a broad Lorentzian of width Ω_f. The two modes (Ω_s and Ω_f, slow and fast, respectively) are given by the following approximate forms:

$$\Omega_s = \left[\frac{1}{\mathcal{D}k^2} + \frac{\mathcal{D}_G}{\mathcal{D}}\lambda_\tau\right]^{-1}, \tag{2.1}$$

$$\Omega_f = \frac{1}{\lambda_\tau} + \mathcal{D}_G k^2, \tag{2.2}$$

where $\mathcal{D}_G$ is the diffusion coefficient of the transient gel, $\mathcal{D}$ is the diffusion coefficient of the solution, and λ_τ is the stress relaxation time. These two modes of the relaxation of the structure factor have also been observed in micellar systems [26,27].

The Helfand-Fredrickson (HF) model examines the effect of shear on the growth, convection, and diffusion of concentration fluctuations. The velocity and stress fields are then perturbed by the nonuniform viscosity. The HF model predicts that the angle-dependent structure factor $S(\bar{k})$ is given by

$$S(\bar{k}) = \frac{k_B T}{\dfrac{\partial^2 f}{\partial c^2} - \hat{k}\hat{k}:\dfrac{\delta \underline{\underline{\sigma}}}{\delta c}}, \tag{2.3}$$

where k_B is the Boltzmann constant, T is the absolute temperature, f is the free energy, c is the concentration, $\hat{k}$ is the unit vector with direction of the wave vector ($\bar{k}$), $\underline{\underline{\sigma}}$ is the stress tensor, and $\frac{\delta \underline{\underline{\sigma}}}{\delta c}$ is the variation in the stress tensor when a concentration perturbation occurs.

The Helfand-Fredrickson model does not consider stress relaxation since their constitutive equation is that of a second-order fluid, appropriate to Rouse dynamics of nonentangled chains.

Milner's model [24,25] employs a constitutive equation written in terms of the strain tensor with a relaxation time for the stress, which leads to two coupled Langevin equations describing the concentration and the stress fluctuations. Within a two-fluid approach, the time scale of generation and decay of concentration fluctuations is predicted to become shorter than the stress relaxation time. Hence, for wave vectors larger than a characteristic wave number k^*, the theory with λ_τ should predict a structure factor $S(\bar{k},\dot{\gamma})$ that decreases with increasing $\bar{k} > k^*$ down to $S(\bar{k},0)$. The model predicts a peak in the structure factor with $\bar{k} \approx k^*$ along the 45° orientation angle, with a peak width of the order of k^*. The presence of this peak in the structure factor is in striking agreement with light-scattering experiments in polymer solutions [28].

Alternative approaches to the coupling of flow and concentration in complex fluids have appeared later. Schmitt *et al.* [21] gave a description of shear-induced transitions (i.e., shear-induced structures or shear-induced phase separation)

and instabilities arising in complex fluids. This model assumes that the chemical potential (μ) in the diffusion equation is a function of both shear rate and concentration, such that the component of the mass flux ($\bar{J}$) can be written as

$$J_2 = -\mathcal{D}\frac{\partial c}{\partial x_2} + \left(\frac{\partial \mu}{\partial \dot{\gamma}_{12}}\right)_{\dot{\gamma}_{12}=\dot{\gamma}_0} \frac{\partial^2 v_1}{\partial x_2^2}, \tag{2.4}$$

where $\mathcal{D}=\partial\mu/\partial c$ and $\gamma_{12}=\sqrt{II_D}$, where II_D is the second invariant of the rate of deformation tensor. In the plane of shear, the following diffusion equation is obtained in terms of the velocity and concentration fluctuations:

$$\frac{\partial \delta c}{\partial t} = \mathcal{D}\frac{\partial^2 \delta c}{\partial x_2^2} + \left(\frac{\partial \mu}{\partial \dot{\gamma}_{12}}\right)\frac{\partial^3 \delta v_1}{\partial x_2^3} \tag{2.5}$$

A local constitutive equation assumes that the shear stress depends on both shear rate and concentration according to

$$\sigma(c,\dot{\gamma}) = \sigma(c_0,\dot{\gamma}_0) + \eta_d \delta\dot{\gamma} + \left[\frac{\partial \sigma}{\partial c}\right]_{c=c_0} \delta c, \tag{2.6}$$

$$\eta_d = \left(\frac{\partial \sigma}{\partial \dot{\gamma}}\right)_{\dot{\gamma}=\dot{\gamma}_0}. \tag{2.7}$$

Upon substitution of Eq. (2.6) into the momentum conservation equation, and allowing fluctuations in the velocity to vary in the x_2-x_3 plane, the following equation for the velocity fluctuations is obtained:

$$\rho\frac{\partial \delta v_1}{\partial t} = \eta_d\frac{\partial^2 \delta v_1}{\partial x_2^2} + \eta_3\frac{\partial^2 \delta v_1}{\partial x_3^2} + \frac{\partial \sigma}{\partial c}\frac{\partial \delta c}{\partial x_2} \tag{2.8}$$

where η_3 is the corresponding viscosity of the gradient in the x_1-x_3 plane. In Fourier space, the following dispersion equation is obtained:

$$\left[\frac{\omega}{k^2}\right]^2 + \left[\frac{\omega}{k^2}\right]\left[\frac{\eta_d}{\rho}\cos^2\theta + \frac{\eta_3}{\rho}\sin^2\theta + \mathcal{D}\right] + \left[\frac{\eta_d}{\rho}\cos^2\theta + \frac{\eta_3}{\rho}\sin^2\theta\right]\mathcal{D} - C\cos^2\theta = 0. \tag{2.9}$$

This equation describes the inhomogeneous shear field and the different orientations of the shear-induced structures or shear-induced phase separation with respect to the shear direction. Here ρ is the density and θ the orientation angle of the wave vector of the velocity perturbation,

$$\bar{k} = \bar{k}_2\cos\theta + \bar{k}_3\sin\theta. \tag{2.10}$$

The coupling term C that arises in Eq. (2.9) is given by:

$$C = \frac{1}{\rho}\left[\frac{\partial \mu}{\partial \dot{\gamma}}\right]_{\dot{\gamma}=\dot{\gamma}_0}\left[\frac{\partial \sigma}{\partial c}\right]_{c=c_0}. \tag{2.11}$$

This coupling term represents the feedback of the different concentrations and viscosities present in the layered solution during shear flow. The type of instability can be determined by the sign of C: if it is positive, the sheared solution is less viscous than the initial one, and if it is negative, the sheared solution is more viscous.

III. MODEL DERIVED FROM EXTENDED IRREVERSIBLE THERMODYNAMICS

The equations of the generalized BMP consist of the upper-convected Maxwell equation for stress coupled to an evolution equation of a scalar representing the flow-induced modifications in the internal structure of the fluid, and to the constitutive equation for the mass flux [29]. The constitutive equation for the stress tensor $\underline{\underline{\sigma}}$ is expressed as

$$\mathfrak{s}_0\overset{\nabla}{\underline{\underline{\sigma}}} + \lambda_\tau\overset{\nabla}{\underline{\underline{\sigma}}} = 2\eta_0\underline{\underline{D}} + \beta_1(\nabla\bar{J})^S. \tag{3.1}$$

Here $\underline{\underline{D}}\equiv(\underline{\underline{L}}+\underline{\underline{L}}^T)/2$ is the symmetric part of rate of strain tensor, $(\nabla\bar{J})^S$ is the symmetric part of the tensor $\nabla\bar{J}$, $\underline{\underline{L}}$ is the rate of strain tensor, $\mathfrak{s}_0=\varphi/\varphi_0$ is the structure parameter representing the internal structure of the fluid that is modified by the flow [φ is the fluidity and ($\varphi_0\equiv\eta_0^{-1}$) is the fluidity at zero shear rate], β_1 is a phenomenological coupling coefficient, and the upper-convected derivative of the tensor $\underline{\underline{\sigma}}$ is defined as

$$\overset{\nabla}{\underline{\underline{\sigma}}} = \frac{d\underline{\underline{\sigma}}}{dt} - (\underline{\underline{L}}\cdot\underline{\underline{\sigma}} + \underline{\underline{\sigma}}\cdot\underline{\underline{L}}^T). \tag{3.2}$$

The evolution equation of a scalar representing flow-induced modifications in the internal structure of the fluid is

$$\frac{d\mathfrak{s}_0}{dt} = \frac{1}{\lambda}(1-\mathfrak{s}_0) + k(\mathfrak{s}_\infty - \mathfrak{s}_0)\underline{\underline{\sigma}}:\underline{\underline{D}} + \beta_3\nabla\cdot\bar{J}. \tag{3.3}$$

The constitutive equation for the mass flux is written as

$$\mathfrak{s}_0\overset{\nabla}{\bar{J}} + \lambda_J\overset{\nabla}{\bar{J}} = -\nabla\mu + \beta_0\nabla\mathfrak{s}_0 + \beta_2\nabla\cdot\underline{\underline{\sigma}}, \tag{3.4}$$

where the upper-convected derivative of the vector $\bar{J}$ is $\overset{\nabla}{\bar{J}} = d\bar{J}/dt - \underline{\underline{L}}\cdot\bar{J}$. Here λ and λ_J are the relaxation time of the internal structure and the mass flux relaxation time, respectively; K is the kinetic constant; β_0, β_2, and β_3 are phenomenological parameters. Equations (3.1), (3.3), and (3.4) together with the conservation equations represent a closed set of time evolution equations for all the independent variables chosen to describe the complex fluid. The mass and momentum conservation equations are

$$\frac{dc}{dt} = -\nabla\cdot\bar{J}, \tag{3.5}$$

$$\rho\frac{d\bar{u}}{dt} = -\nabla p + \nabla\cdot\underline{\underline{\sigma}}, \tag{3.6}$$

$\bar{u}$ is the hydrodynamic velocity, p is the pressure, and $\frac{d}{dt} = \frac{\partial}{\partial t} + \bar{u}\cdot\bar{\nabla}$ is the material time derivative. As suggested in Eq. (2.4), in what follows, $\partial J_2/\partial x_2$ is the only nonzero component of the tensor $(\nabla\bar{J})^S$.

A. First approximation: $\lambda_J \ll \lambda_\tau$ and $\varphi \to \varphi_0$

In Eq. (3.4), it is assumed that the mass flux relaxation time is negligible compared to that of stress. A stability

analysis similar to that of Schmitt *et al.* [21] is carried out to generalize the Newtonian approach using the equations derived from EIT. Hence, the chemical potential is a function of the concentration and velocity gradient, i.e., $\mu=\mu(c,\nabla u)$.

The assumed dependence of the chemical potential on the velocity gradient is justified by the fact that in nonhomogeneous flows the concentration in two regions with different shear rate involves a diffusion process. In this case, Eq. (3.4) can be generalized as follows:

$$\varsigma_0\bar{J}=-\mathcal{D}\nabla c-M\nabla\dot{\gamma}+\beta_0\nabla\varsigma_0+\beta_2\nabla\cdot\underline{\underline{\sigma}}, \tag{3.7}$$

where

$$\left(\frac{\partial\mu}{\partial c}\right)_{T,P}=\mathcal{D},$$

$$\left(\frac{\partial\mu}{\partial\dot{\gamma}}\right)=M.$$

Our linear stability analysis assumes small departures from equilibrium, in the range where $\varphi\to\varphi_0$. In this case, the evolution equation for the structure parameter drops out and the constitutive equations for the mass flux and stress become

$$\bar{J}=-\mathcal{D}\nabla c-M\nabla\dot{\gamma}+\beta_2\nabla\cdot\underline{\underline{\sigma}}, \tag{3.8}$$

$$\overset{\nabla}{\underline{\underline{\sigma}}}+\lambda_\tau\underline{\underline{\sigma}}=2\eta_0\underline{\underline{D}}+\beta_1\nabla\bar{J}. \tag{3.9}$$

Taking the divergence of Eq. (3.8) gives

$$\nabla\cdot\underline{J}=-\mathcal{D}\nabla^2c-M\nabla^2\dot{\gamma}+\beta_2\nabla\cdot\nabla\cdot\underline{\underline{\sigma}}. \tag{3.10}$$

Substitution of Eq. (3.10) into the mass conservation equation gives

$$\frac{\partial c}{\partial t}+\bar{u}\cdot\nabla c=\mathcal{D}\nabla^2c+M\nabla^2\dot{\gamma}-\beta_2Z,\quad Z\equiv\nabla\nabla:\underline{\underline{\sigma}}. \tag{3.11}$$

In the following discussion, we consider two cases: the first case deals with fluctuations in the stress and concentration, neglecting fluctuations of the mean velocity representing the macroscopic flow. The second case addresses the more general situation including fluctuations in the shear rate or velocity.

Defining the perturbations for the concentration and stress around the mean value $\langle\ \rangle$,

$$\delta c=c-\langle c\rangle, \tag{3.12}$$

$$\delta\underline{\underline{\sigma}}=\underline{\underline{\sigma}}-\langle\underline{\underline{\sigma}}\rangle. \tag{3.13}$$

In terms of the fluctuations of concentration and stress, Eqs. (3.9) and (3.11) become

$$\frac{\partial\delta c}{\partial t}+\bar{u}\cdot\nabla\delta c=\mathcal{D}\nabla^2\delta c-\beta_2\delta Z=-\nabla\cdot\delta\bar{J}, \tag{3.14}$$

$$\delta\underline{\underline{\sigma}}+\lambda_\tau\left[\left(\frac{\partial}{\partial t}+\bar{u}\cdot\nabla\right)\delta\underline{\underline{\sigma}}-\nabla\bar{u}\cdot\delta\underline{\underline{\sigma}}-\delta\underline{\underline{\sigma}}\cdot\nabla\bar{u}^T\right]=[2\delta\eta\underline{\underline{D}}+\beta_1\nabla\delta\bar{J}]. \tag{3.15}$$

Taking the double divergence of Eq. (3.15) yields

$$\delta Z+\lambda_\tau\left[\frac{\partial\delta Z}{\partial t}+\bar{u}\cdot\nabla\delta Z\right]=(\nabla\nabla:\underline{\underline{D}})\left(\frac{\partial\eta}{\partial c}\right)\delta c+\beta_1\nabla^2(-\mathcal{D}\nabla^2\delta c+\beta_2\delta Z), \tag{3.16}$$

where the mass conservation, Eq. (3.14), and the following relations have been used:

$$\nabla\cdot\nabla\cdot[\bar{u}\cdot\nabla\delta\sigma_{ij}-(\nabla\bar{u})\cdot\delta\sigma_{ij}-\delta\sigma_{ij}\cdot\nabla\bar{u}^T]=(\bar{u}\cdot\nabla)\delta Z, \tag{3.17}$$

$$\nabla\cdot\nabla^2\bar{J}=\nabla^2(\nabla\cdot\bar{J}), \tag{3.18}$$

$$\delta\eta=\left(\frac{\partial\eta}{\partial c}\right)\delta c. \tag{3.19}$$

Equations (3.14) and (3.16) are the main results of this section. They share the same form of those given in the two-fluid model by Doi and Onuki ([23], Eqs. (6.9) and (6.10)). If in addition, $\beta_1=0$ and $\lambda_\tau=0$, they reduce to

$$\frac{\partial\delta c}{\partial t}+\bar{u}\cdot\nabla\delta c=\mathcal{D}\nabla^2\delta c-\beta_2\delta Z, \tag{3.20}$$

$$\delta Z=(\nabla\nabla:\underline{\underline{D}})\left(\frac{\partial\eta}{\partial c}\right)\delta c, \tag{3.21}$$

which are of the same form as in the Helfand-Fredrickson theory [4]. The structure factor consistent with Eqs. (3.20) and (3.21) is given in Eq. (2.3). This theory predicts an anisotropic growth of the concentration fluctuations. For example, along the line $k_1=k_2$, the decay of δc is slower than that along the lines $k_1=0$ and $k_2=0$. In fact, when $\lambda_\tau(\partial\eta/\partial c)\bar{k}\bar{k}:\underline{\underline{D}}\approx\mathcal{D}k^2$, the structure factor is strongly distorted. It is well known that this theory predicts an angle-dependent scattering intensity $S=S(\bar{k},\dot{\gamma})$, which is maximum when $\bar{k}$ is oriented parallel to the major axis of the tensor $\delta\underline{\underline{\sigma}}/\delta c$ in near-critical solutions of entangled systems. A low shear rates, the solution behaves as a Newtonian fluid and the major axis of $\delta\underline{\underline{\sigma}}/\delta c$ is oriented at 45° with respect to the flow direction. At this direction, there is a trend toward narrowing the concentration region that opposes the broadening in the orthogonal direction due to diffusion, and leads to slower decay of concentration fluctuations.

In the case when the flow is arrested ($v=0$), Eqs. (3.14) and (3.16) become

$$\frac{\partial\delta c}{\partial t}=\mathcal{D}\nabla^2\delta c-\beta_2\delta Z, \tag{3.22}$$

$$\delta Z + \lambda_\tau \left[\frac{\partial \delta Z}{\partial t} \right] = -\beta_1 \nabla^2 \frac{\partial \delta c}{\partial t}. \tag{3.23}$$

Equations (3.22) and (3.23) describe a relaxation process that gives rise to the following dispersion equation in Fourier space:

$$\left[iw + \mathcal{D}k^2 + \frac{iw\beta_1\beta_2 k^2}{1 + iw\lambda_\tau} \right] \delta c = 0. \tag{3.24}$$

The two modes of this dispersion equation are consistent with the slow and fast modes obtained by Brochard-de Gennes [22] [Eqs. (2.1) and (2.2)] provided that $\beta_1 = \mathcal{D}_G$ and $\beta_2 = \lambda_\tau$, where $\mathcal{D}_G$ is the diffusion coefficient of the transient gel. In what follows, this identification of the phenomenological coefficients is considered throughout the paper. By Fourier transformation of Eqs. (3.14) and (3.16) and solving for the concentration fluctuations, the following equation is obtained:

$$\left(\frac{iw(1 + iw\lambda_\tau + \mathcal{D}_G\lambda_\tau k^2) + \mathcal{D}k^2(1 + iw\lambda_\tau) - \lambda_\tau \left(\frac{\partial \eta}{\partial c} \right) \bar{k}\bar{k}:\underline{\underline{D}}}{(1 + iw\lambda_\tau + \mathcal{D}_G\lambda_\tau k^2)} \right) \delta c = 0. \tag{3.25}$$

The dynamic structure factor associated with Eq. (3.25) is the following:

$$S(\bar{k}, w, \dot{\gamma}) = S(\bar{k}) \frac{1 + B^* k^2}{iw[1 + B^* k^2] + \left[\mathcal{D}k^2 + \lambda_\tau \left(\frac{\partial \eta^*}{\partial c} \right) \bar{k}\bar{k}:\underline{\underline{D}} \right]}, \tag{3.26}$$

where $B^* = \frac{\mathcal{D}_G\lambda_\tau}{1+iw\lambda_\tau}$ and $\eta^* = \frac{\eta}{1+iw\lambda_\tau}$.

The corresponding static structure factor is

$$S(\bar{k}, \dot{\gamma}) = S(\bar{k}) \frac{1 + \mathcal{D}_G\lambda_\tau k^2}{\left[\mathcal{D} - \lambda_\tau \left(\frac{\partial \eta}{\partial c} \right) \hat{k}\hat{k}:\underline{\underline{D}} \right]}. \tag{3.27}$$

This equation predicts the presence of a peak in the structure factor, in agreement with the Milner model [25]. Equation (3.27) contains the stress relaxation time, allowing the induction of stresses in the entangled micellar solution before the concentration fluctuations dissipate, as they relax faster than the stress.

The adiabatic approximation assumes that the polymer elastic stress relaxes quickly to a value consistent with a steady state at a given local concentration and shear rate. This approximation breaks down when the time scale for the inception and termination of concentration fluctuations become shorter than the stress relaxation time. According to Milner [25], if the stress responding with a finite response time λ_τ is unable to follow the fast concentration fluctuations at high wave numbers, then the mechanism for the concentration fluctuation growth is less effective than the adiabatic estimate. Then it is necessary to take into account the stress dynamics where the time derivative of the stress is not zero.

The structure factor given in Eq. (3.27) indicates that for wave numbers larger than the magnitude of a characteristic wave vector k^*, corresponding to the crossover of time scales such that

$$\mathcal{D}(k^*)^2 = \lambda_\tau^{-1}, \tag{3.28}$$

concentration fluctuations relax faster than the stress and induce stresses in the entangled micellar network before they dissipate. In fact, Eq. (3.27) reduces to Eq. (2.3) at small wave numbers (adiabatic approximation). Equation (2.3) accounts only for stress-induced diffusion with dependence on the orientation, but not on the magnitude of $\bar{k}$. For large values of the wave number, the structure factor Eq. (3.27) shows a dependence on the magnitude of $\bar{k}$ [see numerator of Eq. (3.27)]. These predictions are in accord with experiments.

It should also be mentioned that the structure factor given in Eq. (3.27) does not include convection. The first contribution of affine convection, as discussed by Milner [25], enhances scattering at 135° and suppresses fluctuations at 45°, exactly opposite to the effect of the term resulting from the concentration dependent viscosity.

B. Transient gel

Finally, even in the absence of shear flow, concentration and stress are dynamically coupled. Equation (3.26) becomes

$$S(\bar{k}, w) = S(\bar{k}) \frac{1 + B^* k^2}{iw[1 + B^* k^2] + \mathcal{D}k^2}. \tag{3.29}$$

This expression gives the dispersion relation corresponding to Eq. (3.24). In transient studies, such as cessation of steady shearing, one can discern both the k-independent viscoelastic time scale associated with the growth of viscoelastic stresses, and the k-dependent diffusive time scale. These time scales are provided by the roots of the dispersion Eq. (3.24). Furthermore, the basic physics inherent in Eq. (3.26) is such that on time scales short compared to the stress relaxation time, the strain responds as if the solution were a gel, with a modulus equal to the plateau modulus. The length scale below, which is an important effect, is given by comparing the rate of solvent diffusion in the concentrate solu-

tion, $\mathcal{D}k^2$, with the stress relaxation time λ_τ. The crossover length scale has been called the "magic length." This argument illustrates that our thermodynamic description is compatible with both, the two-fluid theory and the H-F approach.

C. Fluctuations in the concentration, stress and velocity

We now describe the more general case in which fluctuations in the velocity are considered, in the region where inertia is negligible at low Reynolds numbers. The linear momentum balance for velocity fluctuations is

$$\rho\frac{\partial\delta\bar{u}}{\partial t}=\nabla\cdot\delta\underline{\underline{\sigma}}. \tag{3.30}$$

Taking the divergence of the stress constitutive Eq. (3.9), bearing in mind that the stress is function of the shear rate and concentration, we obtain

$$\nabla\cdot\delta\underline{\underline{\sigma}}+\lambda_\tau\left(\frac{\partial}{\partial t}\nabla\cdot\delta\underline{\underline{\sigma}}\right)=\left[\eta(c)\nabla^2\delta\bar{u}+\left(\frac{\partial\underline{\underline{\sigma}}(c)}{\partial c}\right)\nabla\,\delta c+\mathcal{D}_G\nabla^2\delta\bar{J}\right]. \tag{3.31}$$

By taking the Laplacian in the mass flux constitutive Eq. (3.8) and upon substitution the resulting expression in Eq. (3.31) gives

$$\nabla\cdot\delta\underline{\underline{\sigma}}+\lambda_\tau\left(\frac{\partial}{\partial t}\nabla\cdot\delta\underline{\underline{\sigma}}\right)=\eta(c)\nabla^2\delta\bar{u}+\left(\frac{\partial\underline{\underline{\sigma}}(c)}{\partial c}\right)\nabla\,\delta c+\mathcal{D}_G\{-\mathcal{D}\nabla^2\nabla\,\delta c-M\nabla^2\nabla\,\delta\dot{\gamma}+\lambda_\tau\nabla^2(\nabla\cdot\delta\underline{\underline{\sigma}})\}. \tag{3.32}$$

In simple shear flow only fluctuations in c and u are considered to occur in the (2–3) plane; the dependency of fluctuations along the flow direction is then zero, i.e., $\partial\delta c/\partial x_1=0$, $\partial\delta u_1/\partial x_1=0$. The flow direction component of Eq. (3.32) is

$$(\nabla\cdot\delta\underline{\underline{\sigma}})_1+\lambda_\tau\frac{\partial}{\partial t}(\nabla\cdot\delta\underline{\underline{\sigma}})_1=\eta_2\frac{\partial^2\delta u_1}{\partial x_2^2}+\eta_3\frac{\partial^2\delta u_1}{\partial x_3^2}+\frac{\partial\sigma_{12}}{\partial c}\frac{\partial\delta c}{\partial x_2}+\lambda_\tau\mathcal{D}_G\frac{\partial}{\partial x_2^2}(\nabla\cdot\delta\underline{\underline{\sigma}})_1 \tag{3.33}$$

Summarizing, the set of equations within the linear approximation is

$$\frac{\partial\delta c}{\partial t}=\mathcal{D}\frac{\partial^2\delta c}{\partial x_2^2}+M\frac{\partial^3\delta u_1}{\partial x_2^3}-\lambda_\tau\delta Z \tag{3.11'}$$

$$\delta Z+\lambda_\tau\left[\frac{\partial\delta Z}{\partial t}\right]=\left(\frac{\partial^3u_1}{\partial x_1\,\partial x_2^2}\right)\left(\frac{\partial\eta}{\partial c}\right)\delta c+\mathcal{D}_G\frac{\partial^2}{\partial x_2^2}\frac{\partial\delta c}{\partial t}, \tag{3.16'}$$

$$\rho\left(\frac{\partial\delta u_1}{\partial t}\right)=(\nabla\cdot\delta\underline{\underline{\sigma}})_1, \tag{3.30'}$$

$$(\nabla\cdot\delta\underline{\underline{\sigma}})_1+\lambda_\tau\frac{\partial}{\partial t}(\nabla\cdot\delta\underline{\underline{\sigma}})_1=\eta_2\frac{\partial^2\delta u_1}{\partial x_2^2}+\eta_3\frac{\partial^2\delta u_1}{\partial x_3^2}+\left(\frac{\partial\sigma_{12}}{\partial c}\right)\frac{\partial\delta c}{\partial x_2}+\lambda_\tau D_G\frac{\partial^2}{\partial x_2^2}(\nabla\cdot\delta\underline{\underline{\sigma}})_1. \tag{3.33'}$$

The model of Schmitt *et al.* can be obtained if $\lambda_\tau=0$ and $\mathcal{D}_G=0$. Using the following perturbations in Fourier space, with wave vector $\bar{k}=(0,k\cos\theta\hat{e}_2,k\sin\theta\hat{e}_3)$,

$$\delta u_1=\delta u_0\exp(i\bar{k}\cdot\bar{r}+wt), \tag{3.34}$$

$$\delta c=\delta c_0\exp(i\bar{k}\cdot\bar{r}+wt). \tag{3.35}$$

In Fourier space the above equations can be written as

$$\frac{\partial}{\partial t}\bar{y}=\underline{\underline{A}}\bar{y}, \tag{3.36}$$

where $\bar{y}$ is the vector of dependent variables, namely,

$$\bar{y}=\begin{pmatrix}\delta\dot{\gamma}\\ \delta Z\\ \delta Y_1\\ \delta c\end{pmatrix}\qquad Y_1=\frac{\partial(\nabla\cdot\delta\underline{\underline{\sigma}})_1}{\partial x_2}. \tag{3.37}$$

The stability matrix $\underline{\underline{A}}$ of Eq. (3.36) determines the fate of the fluctuations,

$$\underline{\underline{A}}=\begin{pmatrix}0 & 0 & 1 & 0\\ \dfrac{-\mathcal{D}_GMk^4\cos^2\theta}{\lambda_\tau} & \left(\dfrac{-1+\mathcal{D}_Gk^2}{\lambda_\tau}\right) & 0 & \dfrac{-\mathcal{D}_Gk^4D}{\lambda_\tau}\\ -(\eta_2\cos^2\theta+\eta_3\sin^2\theta)\dfrac{k^2}{\rho\lambda_\tau} & 0 & \left(\dfrac{-1}{\lambda_\tau}-\dfrac{\mathcal{D}_G\lambda_\tau k^2}{\lambda_\tau}\right) & \left(\dfrac{\partial\sigma_{12}}{\partial c}\right)\dfrac{k^2}{\rho\lambda_\tau}\cos^2\theta\\ -Mk^2\cos^2\theta & -\lambda_\tau & 0 & -\mathcal{D}k^2\end{pmatrix}. \tag{3.38}$$

Its eigenvalues obey

$$w_{\bar{k},\alpha}\underline{v}_{\bar{k},\alpha} = \underline{\underline{A}}_{\bar{k}}\underline{v}_{\bar{k},\alpha} \tag{3.39}$$

Here α is the mode index. Following Eqs. (3.38) and (3.39), a positive eigenvalue $w_{\bar{k},\alpha}$ indicates an unstable mode that grows exponentially in time. The eigenvalues $w_{\bar{k},\alpha}$ versus $\bar{k}$ define a multibranched dispersion relation. Two cases are considered for the characteristic polynomial of $\underline{\underline{A}}$. When the scattering angle is zero ($\bar{k}$ is parallel to the velocity gradient),

$$w^4 + w^3\left(\mathcal{D}k^2 + \frac{2}{\lambda_\tau} + 2\mathcal{D}_G\right) + w^2\left(\frac{1}{\lambda_\tau^2} + \frac{2k^2}{\lambda_\tau}[\mathcal{D} + \mathcal{D}_G] + \frac{k^2}{\lambda_\pi \rho}\eta_2 + k^4[\mathcal{D}\mathcal{D}_G + \mathcal{D}_G^2]\right) + w\left(\frac{k^2}{\lambda_\tau^2\rho}[\mathcal{D}\rho + \eta_2] + \frac{k^4\mathcal{D}}{\lambda_\pi\rho}[\mathcal{D}_G\rho + \eta_2] + \frac{k^4\mathcal{D}}{\lambda_\pi\rho}\eta_2 - \frac{Ck^4}{\lambda_\tau}\right) + \frac{k^4\mathcal{D}}{\lambda_\tau^2\rho}\eta_2 - \frac{Ck^4}{\lambda_\tau^2} = 0, \tag{3.40}$$

and when θ is equal to $\pi/2$, i.e., $\bar{k}$ is parallel to the vorticity direction,

$$w^4 + w^3\left(\mathcal{D}k^2 + \frac{2}{\lambda_\tau} + 2\mathcal{D}_G\right) + w^2\left(\frac{1}{\lambda_\tau^2} + \frac{2k^2}{\lambda_\tau}[\mathcal{D} + \mathcal{D}_G] + \frac{k^2}{\lambda_\pi \rho}\eta_3 + k^4[\mathcal{D}\mathcal{D}_G + \mathcal{D}_G^2]\right) + w\left(\frac{k^2}{\lambda_\tau^2\rho}[\mathcal{D}\rho + \eta_3] + \frac{k^4\mathcal{D}_G}{\lambda_\pi\rho}[\mathcal{D}\rho + \eta_3] + \frac{k^4\mathcal{D}}{\lambda_\pi\rho}\eta_3\right) + \frac{k^4\mathcal{D}\eta_3}{\lambda_\tau^2\rho} = 0. \tag{3.41}$$

In Eq. (3.40), $C=(\frac{\partial\sigma_{12}}{\partial c})\frac{M}{\rho}=\frac{1}{\rho}(\frac{\partial\sigma_{12}}{\partial c})(\frac{\partial\mu}{\partial\dot{\gamma}})$ is the coupling parameter defined in the model of Schmitt *et al.* Once again, if $\lambda_\tau=0$, Schmitt *et al.* dispersion Eq. (2.9) is recovered.

The coupling term C represents the feedback of the different concentrations and viscosities that are present in a layered solution during shear flow. The relative viscosity of the sheared solution determines the type of instability. If the sign of the coupling term is positive ($C>0$), the induced phase is less viscous (shear thinning) than the initial one. If ($C<0$), the induced phase is more viscous (shear thickening). In this last case, the diffusion coefficient, $\mathcal{D}$, determines the type of instability because concentration and flow inhomogeneities will develop either parallel to the vorticity direction, $\bar{k}\|e_3$, as found by Fischer *et al.* [30] or parallel to the flow gradient, $\bar{k}\|e_2$, as found by Liu and Pine [31]. As consequence, the coexisting phases experience different stresses but similarly sheared and pure mechanical ($\mathcal{D}>0$) and spinodal ($\mathcal{D}<0$) instability can be observed. Notice that if the angle is 90°, the mechanical and thermodynamic instabilities are decoupled, and hence Eq. (3.41) can be recovered if $C=0$ and write η_3 instead of η_2 in Eq. (3.40).

D. Analytical approximations

The dispersion equation for zero scattering angle (3.40) has four roots, depending on the magnitude of the wave vector. At high frequencies, terms of order w^1 and w^0 can be neglected, resulting in the following asymptotic expressions for large and small k, respectively: For $k\to 0$

$$\omega_{f1} = -1/\lambda_\tau \tag{3.42}$$

and for $k\to\infty$

$$\omega_{f2} = -(\mathcal{D}_G + \mathcal{D})k^2 \tag{3.43}$$

At low frequencies, terms of order w^4 and w^3 are neglected and the following asymptotic limits are obtained: For $k\to 0$

$$\omega_{s1} = -(\mathcal{D} + \eta_2/\rho)k^2 \tag{3.44}$$

and for $k\to\infty$, the slow mode can be obtained from the roots of the following equation:

$$a(\omega\lambda_\tau)^2 + b(\omega\lambda_\tau) + h = 0, \tag{3.45}$$

where

$$a = \mathcal{D}_G(\mathcal{D}_G + \mathcal{D}),$$

$$b = \mathcal{D}_G(\mathcal{D} + \eta_2/\rho) + (\mathcal{D}\eta_2/\rho - C),$$

$$h = \mathcal{D}\eta_2/\rho - C.$$

In the particular case where $C\to 0$ (no coupling), the following root is obtained:

$$\omega_{S2} = -\frac{\left[\left(\mathcal{D} + \frac{\eta_2}{\rho}\right) + \frac{\mathcal{D}}{\mathcal{D}_G}\frac{\eta_2}{\rho}\right]}{\lambda_\tau(\mathcal{D} + \mathcal{D}_G)}. \tag{3.46}$$

If $\mathcal{D}_G \gg \mathcal{D}$ and $\eta_2\to 0$,

$$\omega_{S2} = -\frac{1}{\lambda_\tau}\frac{\mathcal{D}}{\mathcal{D}_G} \tag{3.47}$$

is obtained.

The four roots of the dispersion equation [Eqs. (3.42)–(3.44) and (3.47)] agree with those obtained by Brochard-de Gennes for a transient gel, Eqs. (2.1) and (2.2). This prediction is here shown for the first time, i.e., by introducing stress relaxation in the uncoupled case, the dispersion equation obtained from the generalization of the model of Schmitt *et al.* agrees with the transient-gel model of Brochard–de Gennes. Furthermore, the case of Schmitt *et al.* can be recovered from the dispersion Eq. (3.40) in the limit where the relaxation time tends to zero, i.e., for $k\to 0$,

$$\omega_1 = -(\mathcal{D} + \eta_2/\rho)k^2 \tag{3.44'}$$

and for $k\to\infty$,

$$\omega_2 = -\frac{(\mathcal{D}\eta_2/\rho - C)k^2}{(\mathcal{D} + \eta_2/\rho)} \tag{3.48}$$

The two roots [Eqs. (3.44′) and (3.48)] obtained for the Newtonian limit agree with the instability scheme developed by Schmitt *et al.*, namely:

(a) If C and $\mathcal{D}$ are positive, the first instability appears when $C \geq \eta_2/\rho$ [numerator of Eq. (3.48) is negative-and denominator is positive].

(b) If C is negative and $\mathcal{D}$ positive, the other instability appears when $\mathcal{D}+\eta_2/\rho \leq 0$, with positive numerator in Eq. (3.48). Hence, η_2 should be negative, i.e., a mechanical instability occurs.

(c) If C and $\mathcal{D}$ are negative, Eq. (3.48) marks the instability with η_2 negative or positive. The numerator in Eq. (3.48) is then positive.

In the case of θ equal to $\pi/2$, no coupling exists ($C=0$) and Eq. (3.48) is replaced by

$$k \to \infty,$$

$$\omega_2 = -\frac{\mathcal{D}\eta_3/\rho}{\mathcal{D}+\eta_3/\rho}k^2 \tag{3.49}$$

and hence instabilities appear when both $\mathcal{D}$ and η_3 are negative. They lie along the vorticity axis.

When stress relaxation is included to generalize the model of Schmitt *et al.*, Eqs. (3.42) and (3.43) ensure stability at high frequencies for all wave numbers. In the low-frequency region, Eq. (3.44) is identical to Eq. (3.44′) at low wave numbers, and so instabilities appear when $\mathcal{D}+\eta_2/\rho \leq 0$. At high wave numbers, instead, the fourth root of Eq. (3.45) for $C \neq 0$ and $\mathcal{D}_g \gg \mathcal{D}$ is

$$\omega_{S2} = -\frac{\left[\left(\mathcal{D}+\frac{\eta_2}{\rho}\right)\mathcal{D}_G + \left(\frac{\mathcal{D}\eta_2}{\rho}-C\right)\right]}{\mathcal{D}_G^2\lambda_\tau}. \tag{3.50}$$

Instead of Eq. (3.48), where the terms in parenthesis are divided, in Eq. (3.50) they are summing. Therefore, the instabilities depend not only on the sign of the numerator and denominator, but also on their magnitudes. Since the denominator is always positive, the system is unstable when the numerator becomes negative. The following cases are suggested:

(a)

$$\left(\frac{\mathcal{D}\eta_2}{\rho}-C\right) < 0 \quad \text{and} \quad \left(\mathcal{D}+\frac{\eta_2}{\rho}\right) < 0. \tag{3.51}$$

(b)

$$\left|\mathcal{D}+\frac{\eta_2}{\rho}\right|\mathcal{D}_G < \left|\frac{\mathcal{D}\eta_2}{\rho}-C\right|, \quad \left(\frac{\mathcal{D}\eta_2}{\rho}-C\right) < 0. \tag{3.52}$$

(c)

$$\left|\mathcal{D}+\frac{\eta_2}{\rho}\right|\mathcal{D}_G > \left|\frac{\mathcal{D}\eta_2}{\rho}-C\right|, \quad \left(\mathcal{D}+\frac{\eta_2}{\rho}\right) < 0. \tag{3.53}$$

Accordingly, the criteria for instability holds if $C > \mathcal{D}\,\eta_2/\rho$, together with the following cases:

Case 1: $C>0$, $\mathcal{D}>0$. In this case, the coupling of flow with concentration dominates and (b) applies. Instability occurs in the regions along the flow curve for positive or negative η_2. As shown later in the numerical results, this instability is also present even in the high shear rate region past the plateau. Fluctuations in concentration induce fluctuations in the shear rate, which themselves amplify the concentration fluctuations. Since this term is larger than that representing the mechanical and thermodynamic instabilities, the instability occurs before any spinodal phase separation and in the shear rate range previous to the negative slope that leads to the mechanical instability.

Case 2: $C>0$, $\mathcal{D}<0$. If in addition, $\mathcal{D} > \eta_2/\rho$, case (a) applies and the system is always unstable. In contrast to the Newtonian analysis, case (a) is different. The combination of positive C and negative $\mathcal{D}$ means that the induced phase has lower viscosity but the system is unstable.

Case 3: $C<0$, $\mathcal{D}>0$. In case (c), the mechanical or thermodynamic instabilities decouple, dominating over the coupled instability $\mathcal{D} > \eta_2/\rho$ and occur separately. In this particular case, for the instability to occur, it is necessary that $\eta_2/\rho > \mathcal{D}$ and that η_2/ρ be negative. The instability will be purely mechanical (along the negative slope of the flow curve).

Case 4: $C<0$, $\mathcal{D}<0$. Here (c) holds again. The instability occurs when $\mathcal{D} > \eta_2/\rho$, and it will be of the thermodynamic type. η_2 may be positive or negative, which means that a thermodynamic instability may occur along the entire flow curve. The decoupling coincides with that of a thermodynamic instability and that is positioned along the vorticity direction. Again, in accordance to the Brochard–de Gennes picture, the peak corresponding to the emergence of a structure is absent. Instead, the model predicts metastable regions where the gel is transient, and this prediction agrees with experimental data.

TABLE I. Experimental values of the model parameters for various CTAT concentrations [33,34].

CTAT	2%	5%	10%	20%
φ_0 (Pa s)$^{-1}$	0.06	0.02	0.01	0.004
φ_∞ (Pa s)$^{-1}$	13	11	10	4
k_0 (Pa)$^{-1}$	1×10^{-3}	2×10^{-4}	3×10^{-5}	2×10^{-6}
λ_τ (s)	0.1	0.2	0.3	0.35
ϑ (s)	0.004	0.009	0.01	0.03

IV. NUMERICAL RESULTS: INTRINSIC CONSTITUTIVE CURVE

Cetyltrimethylammonium tosilate (CTAT) is a viscoelastic wormlike micellar solution that presents instabilities under simple shear [32]. The BMP model can predict the associated nonmonotonic constitutive curve under steady simple shear. In this case, Eqs. (3.1) and (3.3) lead to the following expression for the fluidity under homogeneous flow ($\bar{J}=0$):

$$\varphi^2 - \varphi_0\varphi - k_0\lambda(\varphi_\infty-\varphi)\dot{\gamma}_{12}^2(1+\vartheta\dot{\gamma}_{12}) = 0, \tag{4.1}$$

where k_0 is the kinetic constant for structure breakdown and ϑ is the shear-banding intensity parameter. The parameters required to predict the constitutive curve, φ_0, φ_∞, k_0, λ, and ϑ are estimated from separate rheological experiments and from the criterion to set the stress plateau [33]. The values of these parameters (disclosed in Table I) have been reported by

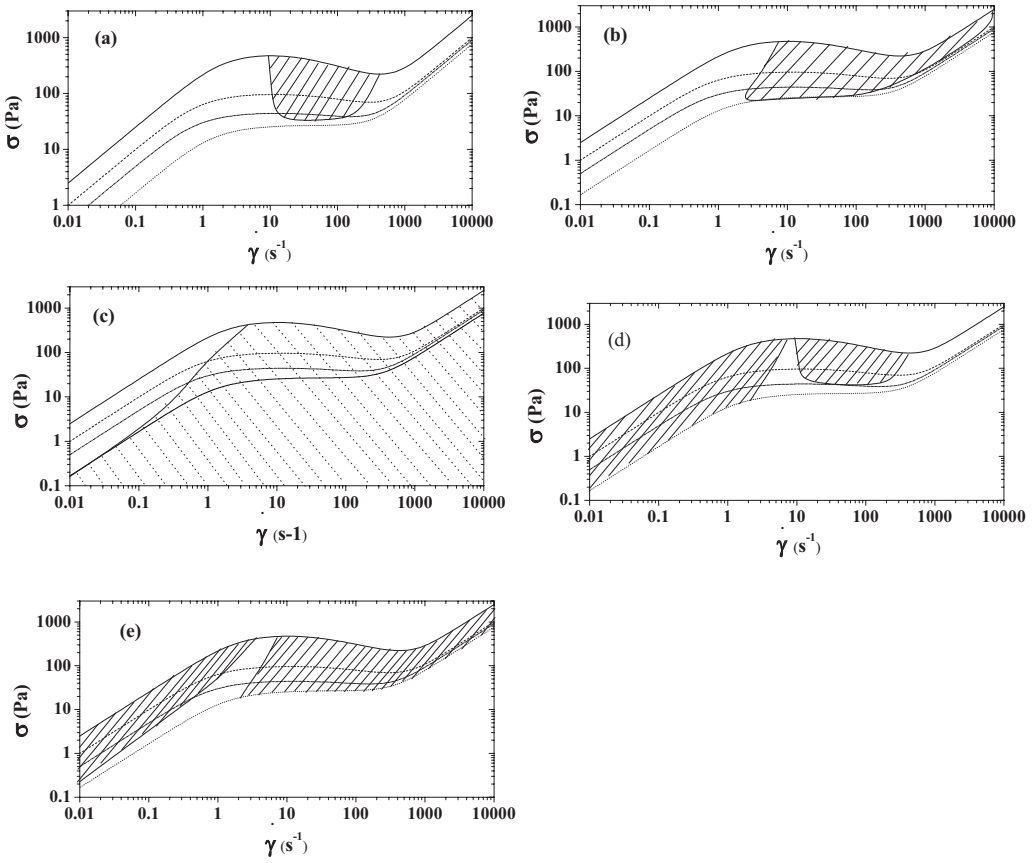

FIG. 1. Intrinsic constitutive curves for 20, 10, 5 and 2 wt. % CTAT solutions. (a) Unstable regions for the uncoupled model. (b) Coupled model, $C=1\times10^{-11}$ and $\mathcal{D}=3.5\times10^{-9}$ (c) Coupled model, $C=1\times10^{-5}$ and $\mathcal{D}=3.5\times10^{-4}$. (d) Coupled model with negative C and $\mathcal{D}$, $C=-1\times10^{-11}$ and $\mathcal{D}=-3.5\times10^{-9}$. (e) Coupled model with negative C and $\mathcal{D}$, $C=-1\times10^{-5}$ and $\mathcal{D}=-3.5\times10^{-4}$. (Units of C are $\mathrm{cm}^4/\mathrm{s}^2$ and those of $\mathcal{D}$ are cm^2/s).

Bautista *et al.* [33] for the CTAT system at various surfactant concentrations.

Equation (4.1) defines a set of intrinsic constitutive curves (dashed lines in Fig. 1), one for each CTAT concentration. The nonmonotonicity of the constitutive curves is determined by the value of the shear banding intensity parameter ϑ, which decreases as the concentration is reduced or the temperature is increased. Along this trend, the region of negative slope narrows, terminating in a critical point at 2 wt. % CTAT. The same qualitative trend has been observed in the cetylpyridium chloride (CPCl)/sodium salycilate (NaSal)/brine/system [33].

A. Results: uncoupled model

To obtain numerical results, the background homogeneous shear state is tracked upwards and downwards sweeping along the intrinsic constitutive curve. The spinodal is determined when the eigenvalue $w^-_{k,\alpha}$ of Eq. (3.39) with the largest real part crosses the imaginary axis in the positive direction. Values of C and $\mathcal{D}$ were chosen considering that a single unstable eigenmode with positive real part is obtained, and for this reason C and $\mathcal{D}$ are first given positives values.

In the uncoupled limit $C=0$, fluctuations in the mechanical variables decouple from the concentration. The instability is mechanical and the spinodal signals the region where the negative slope of the constitutive curve holds.

Figure 1(a) shows the numerical results in the uncoupled case for the spinodal [shaded region in Fig. 1(a)]. For the 5, 10, and 20 wt. % concentrations the unstable zone coincides with the negative slope. The negative region disappears at the critical concentration (2 wt. % CTAT) as expected. This behavior is like those of near-critical systems.

Analytically, the instability can be obtained from Eq. (3.39), written as

$$w_k^4 + a_1 w_k^3 + a_2 w_k^2 + a_3 w_k + a_4 = 0, \tag{4.2}$$

where the a_i $(i=1,\ldots,4)$ are the coefficients of the equation and the independent term is $a_4=\mathrm{Det}\,\underline{\underline{A}}$. The condition for the unstable zones is determined by the sign of the determinant of $\underline{\underline{A}}$, i.e., $\mathrm{Det}\,\underline{\underline{A}}<0$ [19].

$$a_4 = \mathrm{Det}\,\underline{\underline{A}} = \left[\frac{k^4\mathcal{D}}{\lambda_\pi \rho}\right]\eta_2 - \frac{Ck^4}{\lambda_\tau^2}. \tag{4.3}$$

In the uncoupled limit $C=0$, and hence the second term of right-hand side of Eq. (4.3) vanishes. If $\mathcal{D}$ is positive, the condition for instability is determined by the negative value of η_2. Since the sign of η_2 is related with the vanishing derivative of the stress with respect to the shear rate, then the

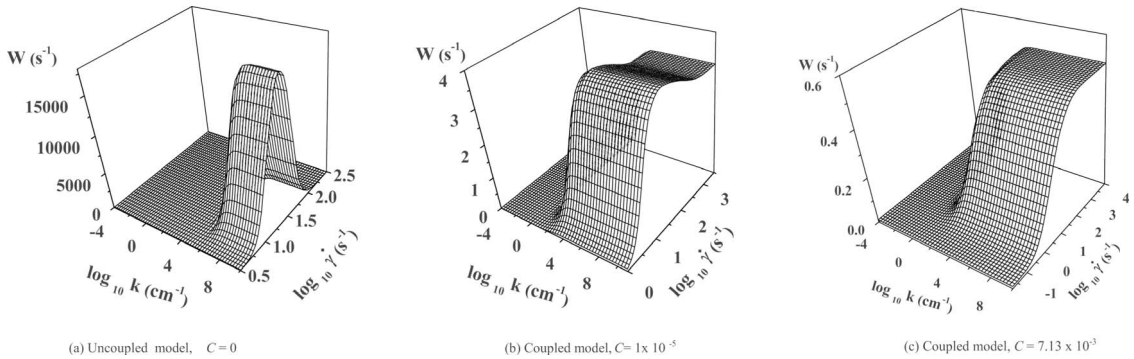

FIG. 2. Dispersion relations for 20 wt. % CTAT for various regimes discussed in the text: (a) Uncoupled model, $C=0$, (b) Coupled model $C=1\times10^{-5}$, (c) Coupled model $C=7.13\times10^{-3}$. Units of C are $\mathrm{cm}^4/\mathrm{s}^2$, $k(\mathrm{cm}^{-1})$, $\dot{\gamma}(\mathrm{s}^{-1})$, $w(\mathrm{s}^{-1})$.

instability appears when the stress in the constitutive curve is decreasing with the shear rate (purely mechanical instability).

B. Dispersion relation

Consideration is now given to the dispersion relation in the unstable region for the uncoupled limit. The dispersion relation was obtained from the eigenvalues of Eq. (4.2). Numerical results show that only one of the four eigenvalues was real and positive in the negative slope region. For pure mechanical instability, the positive dispersion branch is shown in Fig. 2(a) and in Fig. 3 for a 20 wt. % CTAT solution. Figure 3 shows that the growth rate of w tends to zero as $k\rightarrow0$, and tends to a plateau as $k\rightarrow\infty$. This may be understood via the analytical results obtained from the characteristic equation of matrix $\underline{\underline{A}}$ (Eq. (4.2)), and the roots of which have been discussed in the analytical approximations section. The branch at low wave numbers is purely diffusive, in agreement with Eq. (3.44). As the wave number increases, the dispersion curve becomes independent of the wave number, in agreement with Eq. (3.47). Agreement with the analytical approximation (illustrated as a dashed line) is disclosed in Fig. 3.

C. Results: coupled model

For the coupled model ($C\neq0$), the fluctuations of concentration are coupled with the flow. For this case there are two possibilities: $C>0$ and $C<0$. The value of C and $\mathcal{D}$ were assigned considering that only a single unstable eigenmode with positive real part was obtained.

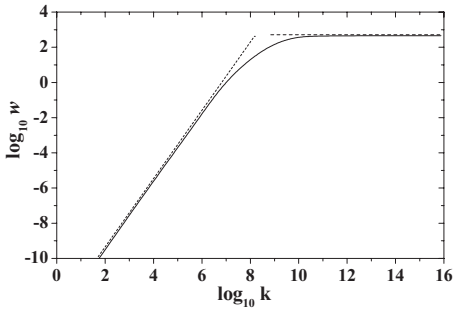

FIG. 3. Dispersion regime for 20 wt. % CTAT solution, $C=0$, $\dot{\gamma}=0.034$ (s^{-1}).

The numerical results are exposed in Figs. 1(b)–1(e). When the value of the parameter C is small, the spinodal is shifted only slightly to lower shear rates [shaded region in Fig. 1(b)], so that the stability in this region is still essentially mechanical. However, a new result is the large unstable region predicted along the second Newtonian branch of the flow curve at high shear rates. When C and $\mathcal{D}$ increase, the shift of the spinodal increases drastically to lower shear rates [shaded region in Fig. 1(c)]. Instability sets in at very low shear rates, within the first Newtonian region, for which the regime of negative constitutive slope is irrelevant. Notice that the instability span is larger as the solution is more diluted.

Results for both positive C and $\mathcal{D}$ imply that the coupled flow-concentration instability occurs along the entire flow curve. Concentration fluctuations induce shear rate fluctuations, which in a feedback process generate an amplification of concentration fluctuations. The sheared solution is less viscous than the initial one and band structures perpendicular to the velocity-gradient direction appear, as found by Liu and Pine [31].

Remarkably, Fig. 1(c) further shows that the second Newtonian region also presents instability for C and $\mathcal{D}$ positive. In this case, the region of instability covers the whole second Newtonian region, the extent of which has not been predicted before.

When the stress is decreasing with shear rate, the instability is mechanical, and the uncoupled model coincides with case 3, i.e., a positive diffusion coefficient but the coupling parameter is negative.

In Figs. 1(d) and 1(e), results for negative C and $\mathcal{D}$ are presented. This situation corresponds to case 4. In Fig. 1(d), besides the region of negative slope, instability regions along the first Newtonian regime for the more concentrated solutions appear. For this case, the second Newtonian region is stable. Hence, regions of higher viscosity are unstable, whereas those with lower viscosity tend to be stable. Since C is negative, the induced phase has higher viscosity, which leads the system to instability. When C and $\mathcal{D}$ increase, instability sets in not only the low shear and more concentrated regimes, but also in the second Newtonian region.

In the case of the CTAT solution considered here, no shear thickening is observed at the concentration ranges given in

Table I, and only it is observed at lower concentrations. The same stability analysis could be performed with the shear-thickening solution, giving rise to a more unstable high viscosity phase (not shown), which would agree with the instability detected by Fischer *et al.* [30]. In this case, shear induces a spinodal phase separation and the layering in this case will be parallel to the vorticity direction.

This latter instability case has been reported by Fischer *et al.* [30] in the aqueous surfactant solution of cetylpyridinium chloride and sodium salicylate, investigated in a transparent strain-controlled Taylor-Couette flow cell. This particular wormlike micellar solution exhibits shear thinning first, at low shear rates, and subsequently, at high shear rates, shear thickening. Once the shear-thickening regime is reached, a transient phase separation of the solution into turbid and clear ringlike patterns oriented perpendicular to the vorticity axis are observed. In the shear-thickening regime, the small-angle light scattering exhibits distinctive butterfly patterns. These and the ringlike patterns oriented perpendicular to the vorticity axis are consequences of the structural changes of the oriented micellar aggregates (flow-induced nonequilibrium phase transition) and can be explained, to our knowledge for the first time, in the context of the present model.

D. Dispersion relation: coupled model

Figures 2(b) and 2(c) show the dispersion relations for two cases of the coupled model. The behavior of the grow rate of w is similar to that of the uncoupled case at constant shear rate, see Fig. 2(a), since, in the low wave-number region the behavior is diffusive, whereas when $k \to \infty$, w tends to a wide plateau. However, the behavior of w against shear rate is different to that of the uncoupled case. The uncoupled model the value of w initially grows with shear rate up to a maximum, after which the value of w begins to decrease with shear rate down to zero, see Fig. 2(a). On the contrary, the coupled model in Fig. 2(b) shows that when $k \to \infty$, w first increases with shear-rate up to a maximum, after which w decreases slightly and never goes down to zero. Instead, w tends to a constant plateau independent of shear rate. In Fig. 2(c) in the regime where $k \to \infty$, w initially grows with shear rate up to a plateau, where w again remains constant independent of shear rate. Interpretation of the uncoupled case resorts to the only possible mechanical instability. This solely appears in the zone where the stress is decreasing with shear rate. For the coupled case two types of instabilities occur, one when the stress is increasing with shear rate, where a feedback process generates an amplification of concentration fluctuations in both the first and second Newtonian regimes. The other instability appears in the regions of higher induced viscosity. In the latter case, shear induces spinodal phase separation in the vorticity direction. These instabilities are the origin of the dispersion relation shown in Figs. 2(b) and 2(c).

V. CONCLUSIONS

In this work, the analysis of instabilities generated by the flow-concentration coupling in wormlike micellar systems is performed with the generalized BMP model, which consists in a set of constitutive relationships derived within the EIT formalism. By assuming that the chemical potential is a function of both the concentration and velocity gradient, a coupling between the concentration and momentum equations is allowed. The generalized BMP model permits a further generalization of the model of Schmitt *et al.* that includes stress relaxation and the diffusion coefficient of the transient gel.

The generalized version of the BMP model allows for couplings between the stress constitutive equation, the equation of mass diffusion, and the evolution equation for the structure variable, in this case, the fluidity. The coupling of flow with concentration arises naturally following the EIT methodology, and further we added the functionality of the chemical potential with both shear rate and concentration to generalize the model of Schmitt *et al.* to systems where stress relaxation is important. The static structure factor was obtained in the velocity-gradient plane, and in particular, the HF adiabatic approximation is recovered as the wave number becomes small. This structure factor describes a peak as the stress relaxation characteristic time becomes comparable to that of the diffusive mechanism at low wave numbers. For high wave numbers, this factor depends on the magnitude of k and it is consistent with that developed by Milner using the two-fluid approach. Moreover, if the flow is arrested, the relaxation of the structure factor leads to the dispersion relation of the transient-gel theory of Brochard–de Gennes. Allowing for fluctuations in the velocity and concentrations in the gradient-vorticity plane, we generalize the approach of Schmitt *et al.* and predict a dispersion relation at high wave numbers which does not goes to zero, but attains a plateau at moderate-to-high shear rates.

As the diffusion coefficient of the gel and the stress relaxation time tend to zero, the adiabatic approximation of the model of Schmitt *et al.* is again recovered. The fact that the Brochard–de Gennes model for the transient gel is recovered in the uncoupled case (see the four roots of the dispersion equation when $C=0$) agrees with the experiments by Fischer *et al.* They observed transient structures being formed inducing layering normal to the vorticity axis. These transient structural patterns within the shear-thickening region correspond to spinodal phase separation in the Schmitt case where both $\mathcal{D}$ and C are negative. The transient nature of the instability (transient gel), together with a nonequilibrium phase transition where the mechanical and thermodynamic instabilities are decoupled, forms a picture that combines the physical intuition of the transient gel with the thermodynamic instability scheme, consisting in layers of fluid normal to the vorticity direction. This constitutes a contribution of the model to the understanding of the presence and generation of instabilities along the vorticity axis.

Numerical results show that in absence of coupling between flow and concentration, the instability is purely mechanical and the spinodal is located around the negative slope region, as expected. But when the flow-concentration coupling is present, three types of instability arise. Besides the purely mechanical instability along the negative slope, the other one occurs when the stress is increasing with the shear rate (first and second Newtonian regions). In this case

there is a feedback process between the concentration fluctuations and shear rate fluctuations, which generates an amplification of concentration fluctuations. The consequence is that the sheared solution is less viscous than the initial one and band structures perpendicular to velocity gradient appear. An exceptionally wide instability region is predicted in the second Newtonian region, the extent of which has not been predicted before.

Finally, instabilities are predicted for negative feedback ($C<0$) and negative diffusion coefficient in the regions of high viscosity, which suggest that the induction of a more viscous phase in a shear-thickening solution can lead the system to instability, in this case, the layering is predicted perpendicular to the vorticity direction. Thin layers with higher viscosity than the initial fluid appear, similar to a spinodal phase separation in the vorticity direction. Since the mechanical and thermodynamic instabilities are uncoupled, the instability observed in the experiments agrees with the transient-gel picture.

The instability analysis exposed here has the ingredients to predict the instability patterns of a shear-thickening solution. This approach will enable a direct comparison with experiments. Results will be presented in a forthcoming publication.

ACKNOWLEDGMENTS

We acknowledge support from CONACYT (The National Science and Technology Council) through the Project No. 100195.

[1] J. D. Goddard, Annu. Rev. Fluid Mech. **35**, 113 (2003).
[2] A. Onuki and K. Kawasaki, Ann. Phys. **121**, 456 (1979).
[3] C. Rangel-Nafaile, A. B. Metzner, and K. F. Wissbrun, Macromolecules **17**, 1187 (1984).
[4] E. Helfand and G. H. Fredrickson, Phys. Rev. Lett. **62**, 2468 (1989).
[5] E. Fischer and P. T. Callaghan, Phys. Rev. E **64**, 011501 (2001).
[6] R. G. Larson, Rheol. Acta **31**, 497 (1992).
[7] P. Fischer, Rheol. Acta **39**, 234 (2000).
[8] J. F. Berret, D. C. Roux, and P. Lindner, Eur. Phys. J. B **5**, 67 (1998).
[9] E. K. Wheeler, P. Fischer, and G. G. Fuller, J. Non-Newtonian Fluid Mech. **75**, 193 (1998).
[10] M. E. Cates, J. Phys. Chem. **94**, 371 (1990).
[11] R. W. Mair and P. Callaghan, Europhys. Lett. **36**, 719 (1996).
[12] F. Bautista, J. M. Santos, J. E. Puig, and O. Manero, J. Non-Newtonian Fluid Mech. **80**, 93 (1999).
[13] J.- F. Berret, Langmuir **13**, 2227 (1997).
[14] N. A. Spenley, X. F. Yuan, and M. E. Cates, J. Phys. II **6**, 551 (1996).
[15] S. Lerouge, J. P. Decruppe, and C. Humbert, Phys. Rev. Lett. **81**, 5457 (1998).
[16] J. P. Decruppe, S. Lerouge, and J. F. Berret, Phys. Rev. E **63**, 022501 (2001).
[17] S. Lerouge, J. P. Decruppe, and J. F. Berret, Langmuir **16**, 6464 (2000).
[18] J. F. Berret and G. Porte, Phys. Rev. E **60**, 4268 (1999).
[19] G. Porte, J. F. Berret, and J. L. Harden, J. Phys. II **7**, 459 (1997).
[20] S. M. Fielding and P. D. Olmsted, Phys. Rev. Lett. **90**, 224501 (2003).
[21] V. Schmitt, F. Lequeux, A. Pousse, and D. Roux, Langmuir **10**, 955 (1994).
[22] F. Brochard and P. G. de Gennes, Macromolecules **10**, 1157 (1977).
[23] M. Doi and A. Onuki, J. Phys. II **2**, 1631 (1992).
[24] S. T. Milner, Phys. Rev. Lett. **66**, 1477 (1991).
[25] S. T. Milner, Phys. Rev. E **48**, 3674 (1993).
[26] I. A. Kadoma and J. W. van Egmond, Phys. Rev. Lett. **76**, 4432 (1996).
[27] P. K. Dixon, D. J. Pine, and X.-l. Wu, Phys. Rev. Lett. **68**, 2239 (1992).
[28] X. L. Wu, D. J. Pine, and P. K. Dixon, Phys. Rev. Lett. **66**, 2408 (1991).
[29] O. Manero, J. H. Pérez-López, J. I. Escalante, J. E. Puig, and F. Bautista, J. Non-Newtonian Fluid Mech. **146**, 22 (2007).
[30] P. Fischer, E. K. Wheeler, and G. G. Fuller, Rheol. Acta **41**, 35 (2002).
[31] C. H. Liu and D. J. Pine, Phys. Rev. Lett. **77**, 2121 (1996).
[32] J. F. A. Soltero, F. Bautista, J. E. Puig, and O. Manero, Langmuir **15**, 1604 (1999).
[33] F. Bautista, J. F. A. Soltero, E. R. Macías, and J. E. Puig, J. Phys. Chem. B **106**, 13018 (2002).
[34] J. F. Berret, D. C. Roux, and G. Porte, J. Phys. II **4**, 1261 (1994).